

Experimental Study of the Electrochemical Impedance Characteristics and Mechanical Properties of High Belite Sulfoaluminate Cement

Shiwei Niu^{1,2}, Xingyi Wang², Jianjian Xing¹, Jindu Li¹, Ruizhen Xie³, Xiangling Bai², Pengju Han^{2,*}

¹ Yellow River Engineering Consulting Co., Ltd., Zhengzhou, 450003, China

² College of Civil Engineering, Taiyuan University of Technology, Taiyuan, 030024, China

³ Mechanics Institute, Jinzhong University, Jinzhong, 030619, China

*E-mail: 13834569544@163.com

Received: 26 October 2022/ Accepted: 3 December 2022/ Published: 27 December 2022

In this paper, a series of electrochemical impedance spectroscopy and compressive strength tests were performed on high belite sulfoaluminate cement with different water-cement ratios. The hydration process of cement materials was analysed according to the generation and development of the impedance curve. Then, the electrochemical impedance spectrum of different hydration times was fitted to obtain electrochemical parameters, and the relationship between electrochemical parameters and mechanical properties was established from the perspective of two electrochemical parameters characterizing pore structure. Furthermore, the influence of different factors on the mechanical properties of cement materials was analysed. The results demonstrated that the water-cement ratio does not change the shape of the Nyquist plot in the cement hydration process. The hydration process can be divided into three stages: early stage, middle stage, and late stage. The porosity decreases with increasing hydration degree, which is manifested as a decrease in the electrochemical parameters α and Q . A novel simple and effective formula is proposed to predict the compressive strength of cement materials considering electrochemical parameters: $f_{cu} = A + B \log \alpha - C \log Q$. Among the experimental factors, the water-cement ratio is essential to its compressive strength, and the effect of small pores is greater than that of large pores.

Keywords: high belite sulfoaluminate cement; electrochemical impedance spectroscopy; hydration process; compressive strength; porosity

1. INTRODUCTION

Along with the strategic goal of the “carbon peaking and carbon neutrality” proposal by the Chinese government, low-carbon environmental protection and energy conservation and emission reduction have become vital philosophies today for cement industry growth [1-3]. High belite sulfoaluminate cement (HBSC) is rapidly becoming a cutting-edge research field in cement production

due to its low energy consumption and low carbon emissions [4-6]. This phenomenon occurs because HBSC is calcined with low-grade raw material and industrial waste residue, and the calcination temperature is lower than that of Portland cement, resulting in conservation of resources and energy [7]. HBSC is a cement with dicalcium silicate (C_2S) and anhydrous calcium sulfoaluminate ($C_4A_3\bar{S}$) as the main minerals, changing the design of Portland cement which has tricalcium silicate (C_3S) as the dominant mineral composition, thus greatly reducing CO_2 emissions [8].

As a new type of cement, HBSC combines the advantages of sulfoaluminate cement and Portland cement, such as rapid setting, early strength, micro expansion, low shrinkage, frost resistance, impermeability and corrosion resistance [9-10]. Currently, the relevant production technology of this cement has been relatively perfect, and it has been applied in some large-scale projects, with immeasurable development prospects. However, research on the hydration mechanism of this cement is still insufficient to fully understand the reasons for its excellent mechanical properties, let alone to establish a relationship between the microscopic mechanism parameters and the macroscopic mechanical properties, which limits its engineering application [11-12].

There are extensive studies about the mechanism of cement hydration, and the approaches used in these mechanism studies are diverse. For example, the calorimeter is a sensitive method to measure the heat of hydration for the study of early hydration, which provides a variety of theories about the early hydration mechanism of cement [13-14]. Then, the morphology of the products of the cement hydration process was examined by scanning electron microscopy (SEM), and many significant outcomes were achieved [15-16]. Furthermore, the mineral composition of hydration products can be characterized by X-ray diffraction (XRD) analysis and Fourier transform infrared spectroscopy (FTIR) [17-18]. However, as damage detection methods, these approaches cannot perform real-time and nondestructive testing of the cement hydration process. As a result of the limitations associated with these approaches, electrochemical impedance spectroscopy (EIS) has been widely applied to investigate the hydration mechanism and mechanical properties of cement materials [19].

EIS applies a small amplitude alternating current signal between the planes at both ends of the specimen and measures its response [20-21] so that the corresponding impedance curve can be collected. The electrochemical parameters are obtained by fitting the measured electrochemical impedance spectrum with an equivalent circuit model [22]. Previous research results demonstrate that the electrochemical impedance spectrum is closely related to the hydration process of cement materials, and the electrochemical parameters can reflect the changes in pore structure during the hydration process, while the pore structure of cement materials is related to its mechanical properties [23-25]. Therefore, EIS provides a powerful approach to study the cement hydration mechanism.

The objective of this paper is to investigate the electrochemical impedance characteristics and mechanical properties of HBSC with different water-cement ratios. Based on the characteristics of the electrochemical impedance spectrum at different hydration times, the whole cement hydration process is analysed, and the electrochemical impedance spectrum is then fitted to obtain the electrochemical parameters. In the remainder of this paper, electrochemical parameters are used to characterize the pore structure of cement materials, and the quantitative relationship between the electrochemical parameters of cement materials and their compressive strength is established.

2. MATERIALS AND METHODS

2.1 Experimental materials

The cement used in this test was HBSC provided by Polar Bear Building Materials Co., Ltd., with a strength grade of 42.5. The particle size of HBSC is distributed mainly between 2 μm and 15 μm , and the average particle size is 9.96 μm , which is much less than that of ordinary Portland cement. The XRD pattern of this cement is shown in Figure 1, and its mineral composition and chemical composition are shown in Table 1 and Table 2, respectively. Normal tap water was used in the test, and there was no other admixture.

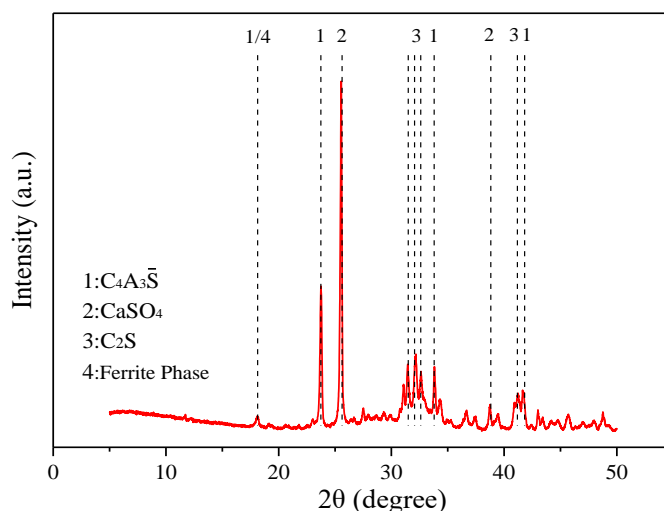


Figure 1. The XRD pattern of HBSC

Table 1. Mineral composition of HBSC

Mineral composition	C_2S	$\text{C}_4\text{A}_3\bar{\text{S}}$	$f\text{-CaSO}_4$	C_4AF	$f\text{-CaO}$
Mass (%)	40.08	34.51	12.27	6.15	2.06

Table 2. Chemical composition of HBSC

Chemical composition	CaO	Al_2O_3	SiO_2	Fe_2O_3	MgO	SO_3	TiO_2	Loss
Mass (%)	51.54	15.34	13.80	1.52	2.08	14.21	0.71	0.38

2.2 Testing methods

The dimensions of the specimens were 70.7 mm \times 70.7 mm \times 70.7 mm, and the water-cement ratios were 0.6, 0.8 and 1.0. The slurry was poured into the mould, and after 24 h of maintenance, the mould was removed and maintained under standard curing conditions (20 ± 2 $^\circ\text{C}$, 95% humidity). The specimens that were maintained to the specified time (Days 1, 3, 7, 14 and 28) were removed for the

electrochemical impedance spectroscopy (EIS) test and then for the mechanical property test. The electrochemical impedance spectrum was measured using a CS350 electrochemical workstation. Copper sheets were fixed at both ends of the specimen as electrodes, and the EIS test was performed in the frequency range of 10^5 Hz to 10^{-2} Hz with a perturbation of 10 mV and a direct current potential of 0.05 V and a minimum high frequency range of 2 mA. The WDW-100 electronic universal testing machine was used for the compressive strength test. The compressive strength test was carried out with reference to the “Test method of cement mortar strength (ISO method)”.

3. RESULTS AND ANALYSIS

3.1 Analysis of Nyquist plots

The electrochemical impedance spectrum involves many different parameters, so it is present in a variety of forms, among which the Nyquist plot is the most frequently adopted [26-27]. In the Nyquist plot, the x-axis represents the real part of the measured impedance, and the y-axis represents the negative number of the imaginary part of the measured impedance, which presents the test results measured at different frequencies on the complex plane. It is suitable for characterizing the essence of the equivalent circuit and reaction process [28]. To analyse the electrochemical impedance characteristics of cement materials, the electrochemical impedance spectrum at the specified time was measured. Then, in accordance with the characteristics of the electrochemical impedance spectrum at different hydration times, the hydration process can be divided into three stages: the early stage, middle stage, and late stage [29]. The electrochemical impedance spectra of cement materials at different hydration stages are shown in Figure 2, Figure 3, and Figure 4. Of these, Figure 2 includes the electrochemical impedance spectrum of hydration time at 1 d, 3 d and 7 d.

In the early stage of hydration, the impedance curves of cement materials with different water-cement ratios are a straight line without the high-frequency semicircle, with a large difference from the quasi-Randles type. Furthermore, their equivalent circuit is a series circuit of resistance and capacitance, illustrating that no visible electrochemical reaction occurred, which is consistent with previous research conclusions [30-31]. This is attributed to the fact that the electrochemical reaction occurs only on the surface of a sufficient amount of hydrated calcium silicate (C-S-H) gel, but the hydration degree of C_2S is still very low at this stage, and only a small amount of C-S-H gel accumulates in the cementitious system, which is not enough for the electrochemical reaction to proceed normally [32].

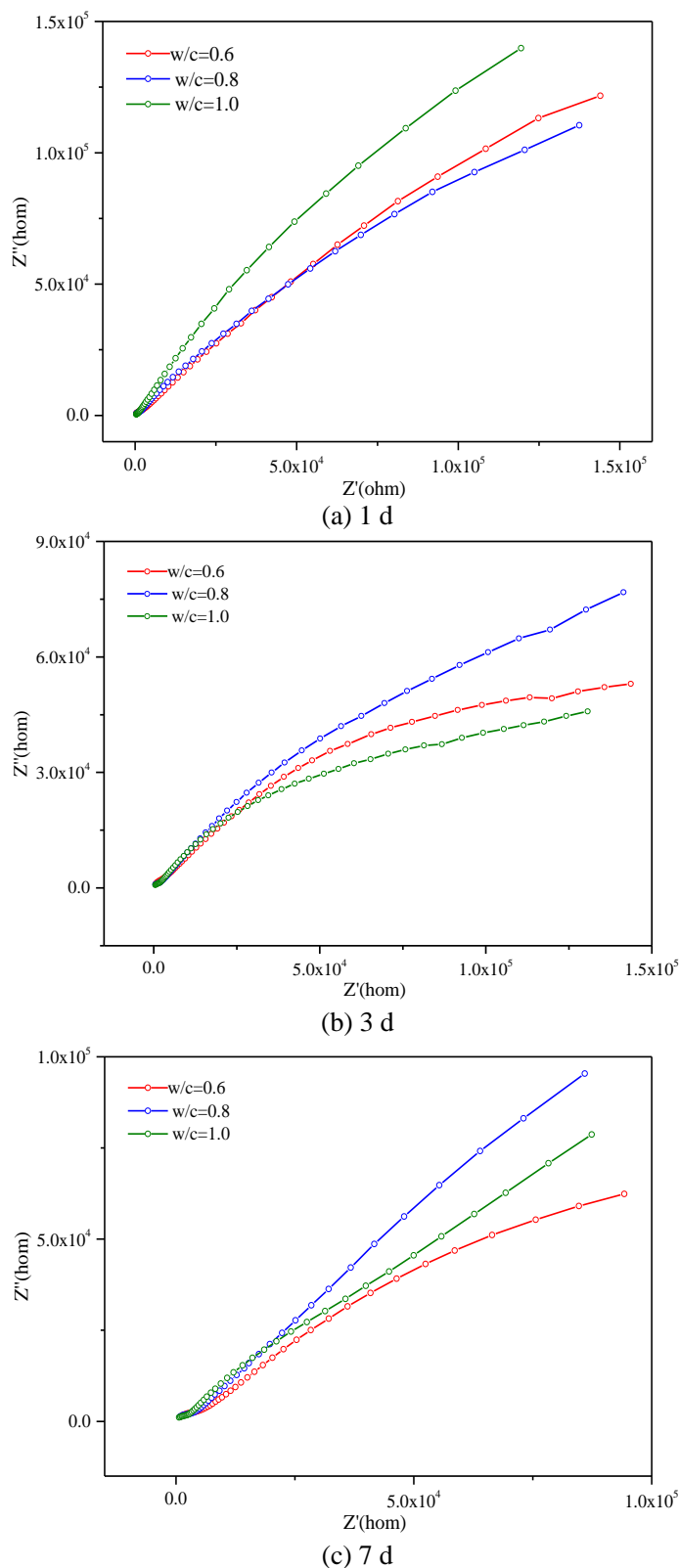


Figure 2. Nyquist plot of the early stage of cement hydration at different times

The Nyquist plot of hydration over 14 d is shown in Figure 3. With the cement hydration progress, the solid phase of supersaturated calcium hydroxide (CH) gradually precipitates out from the pore solution, and a certain amount of C-S-H gel gradually accumulates in the cementitious system so

that the electrochemical reaction can proceed. In the Nyquist plot, the high-frequency region of the impedance curve shows a quasi-Randles characteristic, which is a curve with a certain curvature, and this characteristic will be gradually improved with increasing hydration time. In the low-frequency region, the impedance curve changes from a curve to a straight line that deviates from 45° , with a certain quasi-Randles characteristic [33]. As far as the water-cement ratio is concerned, with the increase in the water-cement ratio, the curvature of the impedance curve in the high frequency region changes significantly, and the diameter of the semicircle decreases, while the slope of the straight line in the low frequency region increases, which suggests that the compactness of the cement materials decreases with the increase in the water-cement ratio [34].

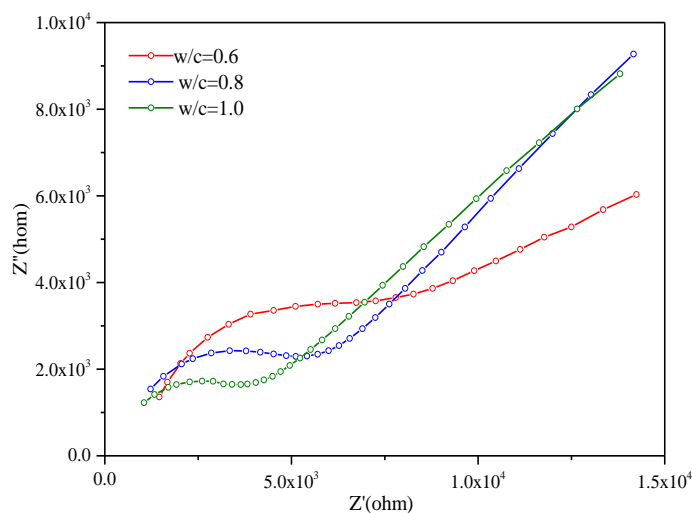


Figure 3. Nyquist plot of cement hydration in the middle stage of 14 d

The Nyquist plot of hydration over 28 d is shown in Figure 4. As the hydration reaches the stabilization period, the impedance curve presents typical quasi-Randles characteristics, with a straight line deviating from 45° at the low frequency region and a flattened semicircle at the high frequency region, which indicates that a considerable amount of C-S-H gel has been accumulated in the cementitious system [35]. Compared with the middle stage of hydration, the curve of the high-frequency region is more significantly curved, and the straight line of the low-frequency region deviates more from 45° . As hydration continues, the impedance curve maintains the quasi-Randles type, but the electrochemical parameters change, which is reflected in the curve as the position and diameter of the semicircle change in the high-frequency region. This phenomenon is caused by the microstructure change of the cementitious system during hydration [36-37]. With the decrease in the water-cement ratio, the diameter of the semicircle in the high frequency region increases, while the slope of the straight line in the low frequency region decreases, which indicates that the porosity of the cement materials decreases, and the structure becomes denser.

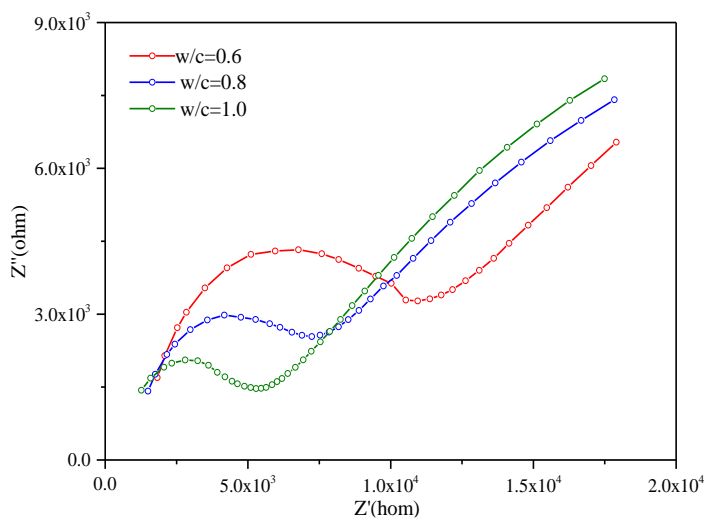


Figure 4. Nyquist plot of cement hydration in the late stage of 28 d

3.2 Analysis of electrochemical parameters

A typical Nyquist plot, due to the particularity of cement materials, is shown in Figure 5. The electrochemical process consists of two parts. The high-frequency region is a deflected semicircle, and its process is controlled by dynamics, while the low-frequency region is a straight line with an inclination angle that deviates from 45° , and its process is controlled by mass transfer. The electrochemical parameters can be obtained by fitting the electrochemical impedance spectrum with an appropriate equivalent circuit model. This paper adopts the typical equivalent circuit model of cement material, namely, the Randles circuit, which can be described as $R_s(C(R_{ct}W))$. The results show that this model has a good fitting degree for the study of cement hydration. Of these, R_s is the resistance of the electrolyte in the pore solution; C is the electric double layer capacitance between the electrolyte solution and the electrode plates; R_{ct} is the charge transfer impedance in the Faraday process; and W is the diffusion process impedance in the Faraday process.

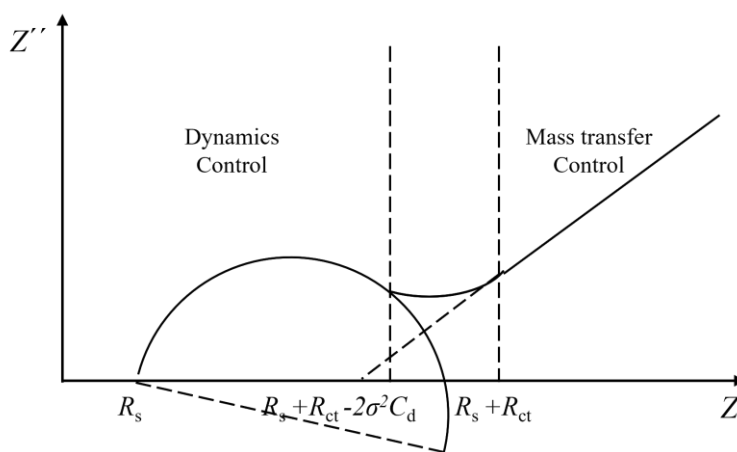


Figure 5. The Nyquist plot (quasi-Randles type)

3.2.1 Electrochemical parameter α

In the high-frequency limit, the impedance curve intersects the y-axis at R_s , which is related to the ion concentration and total porosity of the specimen [38]. As the hydration reaches a certain level, generally after 1 to 2 days, the ion concentration in the pore solution tends to be constant, that is, the electrochemical parameter R_s is determined by the total porosity of the specimen, and the relationship between the two parameters is inversely proportional. In the low frequency limit, only large pores (with a pore size of micrometers or larger) contribute to the capacitance C_d [23], so the value of capacitance C_d reflects the number of large pores in the specimen. From the electrochemical impedance spectrum, the electrochemical parameter α , $\alpha = C_d/R_s$, is selected as a variable to characterize the pore structure of cement materials. For specimens with the same cement type and water-cement ratio, the value of α reflects the contribution of large pores and changes continuously with hydration time. The values of the electrochemical parameters R_s and C_d are shown in Table 3, and the corresponding values of the electrochemical parameter α are shown in Table 4.

Table 3. The values of electrochemical parameters R_s and C_d

Hydration time	C_d (pF)			R_s (Ω)		
	0.6	0.8	1.0	0.6	0.8	1.0
1 d	1161	1189	1215	372	359	348
3 d	1354	1331	1294	516	481	444
7 d	965	867	671	1128	860	556
14 d	1092	918	1010	1562	1225	1052
28 d	864	954	921	1928	1501	1267

Table 4. Values of the electrochemical parameter α

Water-cement ratio	α (pF/ Ω)					
	1d	3d	7d	14d	28d	
0.6	3.12	2.62	0.86	0.69	0.44	
0.8	3.31	2.76	1.01	0.75	0.63	
1.0	3.49	2.91	1.21	0.96	0.72	

As the hydration degree increases, the values of the electrochemical parameter α exhibit a downwards trend, and the extent of the decrease declines. There are two main reasons to explain this phenomenon [39]. First, during the hydration process, the hydration products continuously occupy the pores in the specimen, resulting in a decrease in both the total porosity and the porosity of the large pores, but the decrease rate of the large pore porosity is faster than that of the total porosity. The second is that with the hydration process the pores that can be filled by the hydration products decrease, resulting in the limited decline in total porosity and large pore porosity. Moreover, at the same hydration time, the values of the electrochemical parameter α show an increasing trend with the increase in the water-cement ratio and show the same pattern in the whole hydration process. This is mainly because the pore structure

of cement materials becomes loose with the increase in the water-cement ratio, and the influence of the large pores is also increased [40].

3.2.2 Electrochemical parameter Q

In the low-frequency region, a straight line can be obtained by plotting the real part of the measured impedance Z' with the corresponding $\omega^{-1/2}$ (ω is the angular frequency). Its mathematical expression is shown in Formula (1). The slope Q of the straight line is the diffusion impedance, which is related to the small pores (with a pore size of submicron) and represents the development degree of the connected capillary structure in the specimen [29]. Therefore, the electrochemical parameter Q is used as a variable to characterize the pore structure of cement materials, reflecting the contribution of small pores. For the same cement type and water-cement ratio, the electrochemical parameter Q changes continuously with the hydration process. The values of Q are shown in Table 5.

$$Z' = Q\omega^{-1/2} + K \quad (1)$$

Table 5. The values of electrochemical parameter Q

Water-cement ratio	Q ($k \Omega \cdot s^{-1/2}$)				
	1d	3d	7d	14d	28d
0.6	770	552	282	153	134
0.8	871	675	360	208	147
1.0	959	746	373	255	161

Similar to the variation pattern of the electrochemical parameter α , with increasing hydration degree, the values of the electrochemical parameter Q also show a decreasing trend, and the decreasing extent of their values also decreases. This phenomenon is due to two reasons [41-42]. The first is that with the progress of hydration, the pore structure of cement materials gradually becomes compact, which makes the diffusion resistance increase continuously, and it is difficult for ions to diffuse in the pores. The second is that as the pore structure of cement materials becomes denser, the porosity of small pores decreases accordingly. At the same hydration time, with the increase in the water-cement ratio, the values of the electrochemical parameter Q show an increasing trend in the whole hydration process. This is because the larger the water-cement ratio is, the looser the pore structure of the cement materials is, and the easier the ion diffusion is.

3.3 Relationship between electrochemical parameters and compressive strength

3.3.1 Compressive strength f_{cu}

The electrochemical parameters α and Q are sensitive to changes in the pore structure of cement materials, which is closely related to its mechanical properties [24, 43]. Consequently, this subsection establishes the quantitative relationship between the electrochemical parameters of cement materials and their compressive strength. The values of compressive strength are shown in Table 6.

Experiments show that with hydration progress, the compactness and compressive strength of cement materials increase, and the growth rate of compressive strength in the early period is faster than that in the later period. The reasons for the decrease in the growth rate of compressive strength are as follows: first, the particle size of HBSC is small, resulting in rapid hydration of cement particles [44]; second, as the main mineral component, anhydrous calcium sulfoaluminate has high hydration activity and fast hydration speed [45]; and third, the early hydration products rapidly fill the pores of the specimen, resulting in a great reduction of the pores that can be filled in the later period. As far as the water-cement ratio is concerned, with the decrease in the water-cement ratio, the pore structure of cement materials becomes dense, and its compressive strength increases [39-40, 42].

Table 6. The values of compressive strength f_{cu}

Water-cement ratio	f_{cu} (MPa)				
	1d	3d	7d	14d	28d
0.6	1.79	3.93	5.81	9.64	10.65
0.8	1.41	2.45	4.56	7.82	9.13
1.0	1.27	2.01	3.62	4.79	6.27

3.3.2 Quantitative relationship

The compressive strength of cement materials is related both to large pores and to small pores [23, 38]. Therefore, the assumption is that the compressive strength f_{cu} of cement materials is a functional form of the electrochemical parameters α and Q that characterize its pore structure, as shown in Formula (2). Then, the partial differential equation of the compressive strength f_{cu} is established, as shown in Formula (3).

$$f_{cu} = F(\alpha, Q) \tag{2}$$

$$df_{cu} = \left(\frac{\partial f_{cu}}{\partial \alpha} \right)_Q d\alpha + \left(\frac{\partial f_{cu}}{\partial Q} \right)_\alpha dQ \tag{3}$$

Many previous studies have demonstrated that $\left(\frac{\partial f_{cu}}{\partial \alpha} \right)_Q$ and $\left(\frac{\partial f_{cu}}{\partial Q} \right)_\alpha$ have a linear relationship with $1/\alpha$ and $1/Q$, respectively; that is, the change rate of f_{cu} with α and Q is linear with $1/\alpha$ and $1/Q$,

respectively [22, 41, 46]. Furthermore, analysing the experimental data shows that the two parameters change in opposite directions and the change rate of f_{cu} with α is positively correlated with $\frac{1}{\alpha}$, while the change rate of f_{cu} with Q is negatively correlated with $\frac{1}{Q}$. Therefore, Formula (4) can be derived as follows, and Formula (5) can be derived by combining Formula (3) and Formula (4).

$$\frac{\partial f_{cu}}{\partial \alpha} = \frac{B}{\alpha}, \quad \frac{\partial f_{cu}}{\partial Q} = -\frac{C}{Q} \tag{4}$$

$$f_{cu} = A + B \log \alpha - C \log Q \tag{5}$$

In Formula (5), the three constants A, B and C represent the weight of the influence of experimental factors on the compressive strength f_{cu} , in which A represents the influence of the water-cement ratio, B represents the influence of large pores, and C represents the influence of small pores [41, 47]. The values of the constants of the cement materials are obtained by fitting all experimental data and taking the average value, as shown in Table 7.

Table 7. The values of constants under different water-cement ratios

Constant	A			B			C		
Water-cement ratio	0.6	0.8	1.0	0.6	0.8	1.0	0.6	0.8	1.0
Value	59.8	39.3	28.8	9.1	3.9	4.3	21.9	13.6	9.9

Analysis of the constant data found that the water-cement ratio has the greatest impact on the compressive strength of cement materials, which is shown by the fact that the value of A is far greater than that of B and C. At the same water-cement ratio, the value of C is greater than that of B, and the variation extent of the Q value is much wider than that of α , so the effect of small pores on the compressive strength of cement materials exceeds that of large pores, which is consistent with previous research conclusions [41, 48-49]. With the increase in the water-cement ratio, although the values of the three constants all decrease, the changes are roughly equal in proportion, and only the influence of B on the compressive strength changes significantly, that is, the large pores. It is noteworthy that some studies have proposed that C is a universal constant that does not vary with the cement type and material mix ratio, which is inconsistent with the conclusion in this paper [22, 41, 50]. This is mainly because the three kinds of cement used in the previous study are Portland series cement, with only the amount of admixture changed and not the type of cement, while the HBSC used in this paper is significantly different from Portland cement.

To verify the validity of Formula (5), the linear equation ($y = a + bx$) is used to fit the measured compressive strength and predicted compressive strength of cement materials. The fitting results are shown in Figure 6. The correlation coefficients (R^2) of the fitting equations are all greater than 0.94, indicating that there is a significant correlation between these two parameters. Therefore, Formula (5) is suitable for predicting the compressive strength of HBSC, which establishes the quantitative relationship between the compressive strength and the electrochemical parameters.

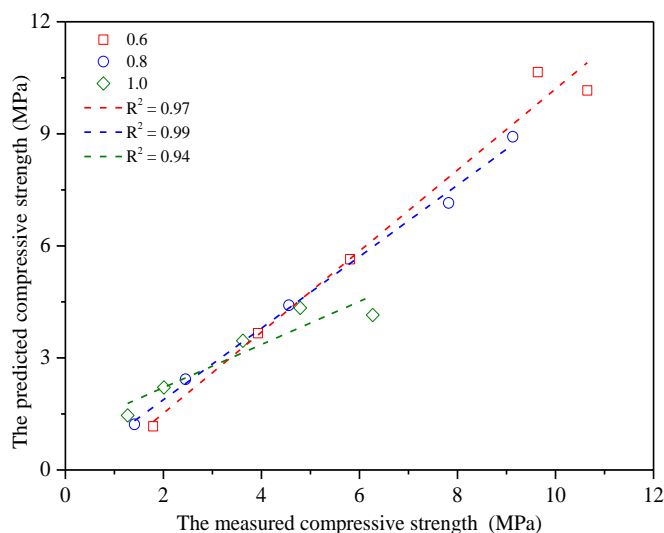


Figure 6. Fitting curves between the measured compressive strength and predicted compressive strength

4. CONCLUSIONS

In this paper, the electrochemical impedance characteristics and mechanical properties of HBSC with different water-cement ratios were experimentally studied. The main conclusions are as follows.

(1) The shape of the impedance curve of cement materials does not change with the change in the water-cement ratio. According to the characteristics of the electrochemical impedance spectrum at different hydration times, the cement hydration process can be divided into three stages: early stage, middle stage, and late stage.

(2) The electrochemical impedance spectra of cement materials with different water-cement ratios have similar variation patterns. In the early stage, there is no electrochemical reaction, and the high frequency region is a straight line, while in the middle stage, the high frequency region is a curve, showing the characteristics of quasi-Randles. In the late stage, the impedance curve is relatively perfect, and the Nyquist plot maintains the quasi-Randles type.

(3) During the entire hydration process, the electrochemical parameters α and Q decrease with increasing hydration time, and the extent of the decline shows a decreasing trend; that is, the total porosity decreases, the porosity of large pores also decreases, and the rate of large pore porosity decline is faster than the total porosity. This can be considered the reason for the increase in compressive strength with the increase in hydration degree.

(4) A prediction formula of compressive strength considering the influence of electrochemical impedance parameters α and Q characterizing pore structure, $f_{cu} = A + B \log \alpha - C \log Q$, is proposed which can effectively predict the compressive strength of cement materials.

ACKNOWLEDGMENTS

The author would like to express his sincere gratitude to Professor Jindu Li and Professor Pengju Han for their guidance, support, and encouragement. The author also thanks the Yellow River Engineering Consulting Co., Ltd. for its financial support and Taiyuan University of Technology for its experimental conditions.

References

1. Z.P. Yang, J.F. Yang, S. Bo, Y.T. Niu, Z.Z. Yong, K.J. Wu, C.J. Zhang, X.Y. Qiao and Y.Y. Zhang, *Constr. Build. Mater.*, 328 (2022) 12699.
2. T. Strunge, P. Renforth and M.V. Spek, *Commun. Earth Environ.*, 1(3) (2022) 3900.
3. E. Crossin, *J. Clean. Prod.*, 95 (2015) 101.
4. S.W. Niu, F.N. Sun, R.Z. Xie, B. He, F.L. Ma, X.A. Guo, A.A. Fattah, X.Y. Wang and P.J. Han, *Int. J. Electrochem. Sci.*, 15(12) (2020) 12264.
5. M.Z. Lan, B.F. Xiang, J. Zhou, Z.X. Ge and C.J. Liu, *J. Chin. Ceramic. Soc.*, 36(8) (2017) 2720.
6. E. Costa and B.D. Eugênio, *Constr. Build. Mater.*, 122(9) (2016) 373.
7. W.L. He, R. Li, Y. Zhang and D.P. Nie, *Constr. Build. Mater.*, 326 (2022) 126672.
8. C. Liu, J.L. Luo, Q.Y. Li, S. Gao, Z.Q. Jin, S.C. Li, P. Zhang and S.C. Chen, *Constr. Build. Mater.*, 228 (2019) 16798.
9. Q. Wang, S.Y. Li, S. Pan and X.M. Kong, *J. Build. Mater.*, 23(2) (2020) 239.
10. X.A. Guo, A.A. Fattah, S.W. Niu, P.J. Han and R.Z. Xie, *Sci. Techno. Eng.*, 21(11) (2021) 4584.
11. L.H.J. Martin, F. Winnefeld, C.J. Müller and L. Barbara, *Cem. Concr. Compos.*, 62 (2015) 204.
12. C.W. Hargis, A. Telesca and P.J.M. Monteiro, *Cem. Concr. Res.*, 65(11) (2014) 15.
13. E. Maruya, E. Sakai, S. Hagiwara and M. Daimon, *J. Adv. Concr. Technol.*, 7(3) (2009) 367.
14. Y.M. Yu, J.F. Hou, Z.Q. Dong, C. Wang, F.Z. Lu and P.A. Song, *J. Fire. Sci.*, 34(3) (2016) 199.
15. Y. Zhang, M.F. Liang, Y.D. Gan and Ç. Oğuzhan, *Mater.*, 15(18) (2022) 6347.
16. C. Rößler, D. Zimmer, P. Trimby and H.M. Ludwig, *Cem. Concr. Res.*, 154 (2022) 106721.
17. K.P. Kunal, D.P. Steven, B. Ali, S. Carmen and B. Oral, *Constr. Build. Mater.*, 158 (2018) 574.
18. E. Kuzielová, M. Slaný, M. Žemlička, J. M Másilko and M.T. Palou, *Cem. Mater.*, 14(11) (2021) 2786.
19. X. Luo, S.J. Li, Z.H. Guo, C. Liu and J.M. Gao, *J. Build. Eng.*, 61 (2022) 105327.
20. T. Pajkossy and R. Jurczakowski, *Curr. Opin. Electrochem.*, 1(1) (2017) 53.
21. M. Cabeza, M. Keddami, X.R. Novoa, I. Sanchez and H. Takenouti, *Electrochim. Acta*, 51 (2006) 8.
22. M.L. Shi and Z.Y. Chen, *J. Build. Mater.*, 1(1) (1998) 30.
23. B.Q. Dong, G. Li, J.C. Zhang, Y.Q. Liu, F. Xing and S.X. Hong, *Constr. Build. Mater.*, 149 (2017) 467.
24. A. Guerrero, A. María, M. Gutiérrez and Ruby, *Constr. Build. Mater.*, 193 (2018) 518.
25. C. Li, Y.F. Fan and Q.C. Li, *J. Build. Mater.*, 23(4) (2020) 755.
26. P. Gu, P. Xie, J.J. Beaudoin and R. Brousseau, *Cem. Concr. Res.*, 23(1) (1993) 157.
27. G.L. Song, *Cem. Concr. Res.*, 30 (2000) 1723.
28. F. Bullerjahn, E. Boehm-Courjault, M. Zajac, H.M. Ben and K. Scrivener, *Cem. Concr. Res.*, 116 (2019) 1208.
29. J.C. Zhang, B.Q. Dong, S.X. Hong, X.J. Teng, G. Li, W.W. Li, L.P. Tang and F. Xing, *Constr. Build. Mater.*, 222 (2019) 41.
30. X.Z. Yuan, Q.L. Liu, W.T. Xu and Y.Z. Tian, *Int. J. Electrochem. Sci.*, 14(12) (2019) 10797.
31. F.J. Jiang, J.X. Gong and W. Zhang, *J. Xi'an Univ. Arch. & Technol. (Nat. Sci. Edi.)*, 48(4) (2016) 493.
32. S.W. Niu, P.J. Han, F.N. Sun, R.Z. Xie, B. He, F.L. Ma, X.A. Guo and A.A. Fattah, *Int. J.*

- Electrochem. Sci.*, 15(9) (2020) 9428.
33. M.Y. Hang, M.H. Jiang, J.W. Xu, T. Cheng, H. Wang and G.M. Zhou, *Sci. Eng. Compos. Mater.*, 28(1) (2021) 352.
 34. J.C. Zhang, F. Zheng, Z.M. Liu, S.X. Hong, B.Q. Dong and F. Xing, *Measurement*, 185 (2021) 109884.
 35. F.J. Jiang, J.X. Gong and H. Wang, *J. Xi'an Univ. of Arch. & Technol. (Nat. Sci. Edi.)*, 51(5) (2019) 582.
 36. S.W. Tang, X.H. Cai, Z. He, W. Zhou, H.Y. Shao, Z.J. Li, T. Wu and E. Chen, *Constr. Build. Mater.*, 146 (2017) 15.
 37. B.Q. Dong, J.C. Zhang, Y.Q. Liu, G.H. Fang, Z. Ding and F. Xing, *Constr. Build. Mater.*, 113 (2016) 997.
 38. G.J. Gu and H.L. Song, *Int. J. Electrochem. Sci.*, 15(12) (2020) 12291.
 39. X.P. An, C.J. Shi, F.Q. He and D.H. Wang, *J. Chin. Ceramic Soc.*, 40(7) (2012) 1059.
 40. Y. Li, Y. Gao, X.T. Zheng and F.Z. Wang, *J. Perform. Constr. Facil.*, 35(5) (2021) 1625.
 41. M.L. Shi, X. Zhang, P.J. Li and L.Y. Jiang, *Bull. Chin. Ceramic Soc.*, 34(4) (1999) 14.
 42. B.Q. Dong, Q.W. Qiu, J.Q. Xiang, C.J. Huang, X. Feng and N.X. Han, *Mater.*, 7(1) (2014) 218.
 43. V.D. Ho, C.T. Ng, C.J. Coghlan, A. Goodwin, C.M. Guckin, T. Ozbakkaloglu and D. Losic, *Constr. Build. Mater.*, 234 (2020) 117403.
 44. J. Neubauer, T. Sowoidnich, L. Valentini, C. Schulbert, C. Naber, C. Röbler, J. Dasilva and F. Bellmann, *Cem. Concr. Res.*, 156 (2022) 106769.
 45. R. Sivakumar, H. Ben and S. Prannoy, *Cem. Concr. Compos.*, 112 (2020) 103694.
 46. C. Xie, Q.C. Wang, S. Li and B. Hui, *Bull. Chin. Ceramic Soc.*, 34(12) (2015) 3695.
 47. L. Chi, Z. Wang, S. Lu, D.Z. Zhao and Y. Yao, *Constr. Build. Mater.*, 208 (2019) 659.
 48. C.W. Song, G.T. Hong and S.C. Choi, *Constr. Build. Mater.*, 265 (2020) 120318.
 49. H.X. Li, Z. Xue, H. Liang, Y.C. Guo, G.W. Liang, D.Y. Ni and Z.H. Yang, *J. Build. Eng.*, 41 (2021) 102780.
 50. S.H. Liu, B. Liu, Y.C. Yao, P. Dong and S.C. Zhao, *J. Wuhan Univ. Technol. (Mat. Sci. Edi.)*, 31(5) (2016) 965.